



Zeeman-ladder analysis of the Raman magnon energies in the quasi-one-dimensional antiferromagnet RbCoCl₃

M. G. Cottam ^{*}

Department of Physics and Astronomy, University of Western Ontario, London, Ontario N6A 3K7, Canada

D. J. Lockwood 

Metrology Research Centre, National Research Council, Ottawa, Ontario K1A 0R6, Canada

 (Received 6 October 2021; revised 25 January 2022; accepted 26 January 2022; published 7 February 2022)

Interest in the spin- $\frac{1}{2}$ hexagonal perovskites, typified by CsCoCl₃ and including RbCoCl₃, has persisted over several decades due to their unusual Ising-chain-like antiferromagnetic ordering. Despite considerable theoretical and experimental work, evidence of the origin of the magnetic excitations of these materials has been limited by an incomplete knowledge of their magnetic ordering and exchange interactions. Now, with the availability of detailed measurements of such information obtained by neutron scattering [M. Mena *et al.*, *Phys. Rev. Lett.* **124**, 257201 (2020)], we are motivated to report a study for RbCoCl₃. We employ the concept of a Zeeman ladder of magnetic excitations below the antiferromagnetic transition temperature at 28 K, as well as showing the existence of a bound magnetic state, to accurately predict the energies of five magnetic excitations observed by Raman scattering. Such a remarkable match of theory to experiment with just one adjustable parameter augers well for theoretical applications in other such perovskites.

DOI: [10.1103/PhysRevB.105.064411](https://doi.org/10.1103/PhysRevB.105.064411)

I. INTRODUCTION

There has been strong interest in recent years regarding the novel properties of hexagonal perovskite compounds such as CsCoCl₃, which have been found to exhibit a quasi-one-dimensional antiferromagnetic ordering at low temperatures as a result of Ising model exchange interactions occurring along the chains of magnetic ions. Features of interest include spin-wave energy continua and the possibility of bound magnon states and their potential applications in spin- $\frac{1}{2}$ quantum-wire transport devices. Most of these transition metal perovskites exhibit two magnetic phase transitions denoted by T_{N1} and T_{N2} . The higher of these transition temperatures T_{N1} represents the temperature below which there is antiferromagnetic ordering in one dimension (1D) along the chains, whereas the lower temperature T_{N2} signifies the onset of an additional 3D interchain ordering.

A large quantity of neutron scattering work, as well as optical measurements such as Raman scattering and far-infrared spectroscopy, for these compounds has been used to determine their structural and dynamic properties. These experimental studies include, for example, CsCoCl₃ (see, e.g., [1–5]), RbCoCl₃ [6–9], TiCoCl₃ [10], and CsCoBr₃ [2–4,11–13]. Often, because of a lack of sufficient resolution, the elastic and inelastic neutron scattering measurements failed to provide sufficient details of the nature of the magnetic ordering, especially for temperatures below T_{N2} . On the other hand, although the optical work often had sufficient resolution to determine the energies of magnetic excitations for small wave vectors,

the lack of detailed information on the spin alignments handicapped the interpretation of the optical results. The case of RbCoCl₃ affords a classic example of this conduct [7] and is the focus of our present work.

The first significant theoretical work on these compounds was due to Villain [14], who proposed a model of an antiferromagnetic chain of spins with a nearest-neighbor exchange acting along the Co chains. The interactions were taken as Heisenberg with an Ising-like anisotropy, and there was no interchain coupling included. Rather than conventional spin-wave theory being employed (because of the low dimensionality and the low spin $S = \frac{1}{2}$), he considered spin-reversal processes, which are equivalent to domain wall production, from which wavelike states were then formed. These developments led to the prediction of a continuum band of magnons [14,15] with the possibility of a bound magnon [16] arising from effects of the next-nearest-neighbor chain interactions. Another important finding [4,17] was that the inclusion of the small exchange interactions between the chains (conventionally described in terms of a staggered field h) led to a discretization of the magnon continuum through a so-called Zeeman “ladder” of energy levels.

Recently, some high-resolution neutron scattering studies of both the magnetic structure [18] and the spin dynamics [19] of RbCoCl₃ have been reported. These results are of sufficient quality to motivate a reassessment of the optical observations in this hexagonal perovskite. Accordingly, we reexamine the detailed optical observations [7–9] of magnetic excitations in this material for temperatures ranging from below T_{N2} (≈ 12 K) and ranging up to T_{N1} (≈ 28 K) and interpret them with the aid of a revised theory based on the foundations established in the earlier work reviewed above. By contrast

^{*}cottam@uwo.ca

with previous Raman studies, we find that a suitably modified theory now provides an excellent account for the origins of all five magnetic excitations observed by Raman scattering [7] for low wave vectors. The modified theory makes use of the Zeeman ladder and the bound magnon state in an analytic formulation. The mechanism giving rise to the one-magnon inelastic light scattering in these antiferromagnetic compounds is taken to be the usual magneto-optical coupling (see, e.g., [20]); the novelty is regarding the magnetization dynamics in these low-dimensional structures.

This paper is organized as follows. In Sec. I we present an account of the relevant Raman spectroscopy results, based on experiments by Lockwood *et al.* [7]. This is followed in Sec. II by an account of the analytic theory, and then in Sec. III an analysis of the magnon modes is presented showing excellent results of a comparison between theory and experiment. The conclusions and some future directions are given in Sec. IV.

II. MAGNON RAMAN RESULTS

The Raman measurements were performed on a single crystal of dark-blue colored RbCoCl₃. The sample was mounted in a Thor S500 continuous-flow cryostat, where the crystal temperature could be controlled to within 0.1 K. The Raman scattering spectra were excited with 50 mW of 476.5 nm argon laser light, analyzed with a Spex 14018 double monochromator at a spectral resolution of 1.4 cm⁻¹, and detected with a cooled RCA 31034A photomultiplier. The Raman signal was recorded at right angles to the incident light in a $X(\dots)Y$ scattering geometry, where the Y axis was chosen to be normal to the crystal (11 $\bar{2}$ 0) cleavage plane and the Z axis was along the crystal c axis.

From symmetry considerations, the magnetic excitations in RbCoCl₃ can be expected to be observed in (ZX) polarization [7,21]. Three vibrational modes of E_{2g} symmetry can also be observed in this polarization [7,22]. These Raman selection rules need to be considered when implementing the Raman measurements. Although the original Raman study of RbCoCl₃ was very comprehensive [7], we need only consider here a subset of results possessing the appropriate polarization. We chose the $X(ZX)Y$ scattering geometry, but also used the $X(ZX + ZZ)Y$ scattering configuration to record weaker Raman scattering from the magnetic excitations at temperatures below T_{N1} . The latter case was achieved by removing the polarization analyzer for those measurements. The inclusion of the $X(ZZ)Y$ spectrum in this case is not a concern, as this spectrum is very weak in the 100 cm⁻¹ region. The results obtained for the mode strengths shown later have been corrected by an intensity difference factor of 0.82 to allow for this difference in scattering geometries. The sample temperatures reported here, by comparison with those reported in Ref. [7], have been corrected for a laser heating of 8 K, which was determined from a preliminary analysis of the temperature dependencies of the magnon peak parameters, where the nominal values of T_{N1} and T_{N2} were recorded as 20 K and 4 K, respectively.

To enable a more detailed analysis of the variation in the spectrum with temperature, the magnon peak parameters were obtained by curve-resolving the spectrum with a number of

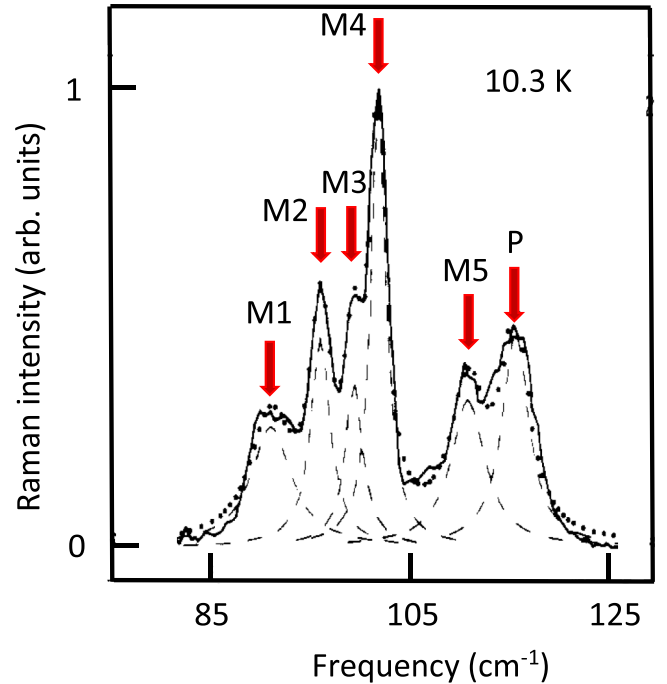


FIG. 1. Raman scattering spectrum (solid line) of intensity versus frequency shift in the region of one-magnon excitation, measured at $T = 10.3$ K and in $X(ZX + ZZ)Y$ polarization. The fitted magnon peaks (see the text) are labeled {M1, M2, ..., M5} and a partially overlapping phonon peak is labeled P. The individual fits and the combined fits are shown by the dashed and dotted lines, respectively.

damped harmonic oscillators of the form

$$I(\omega) = \{\bar{n}(\omega) + 1\} \frac{\mathcal{S}\omega_0^2\gamma^2\omega}{(\omega^2 - \omega_0^2)^2 + \omega^2\gamma^2}, \quad (1)$$

where \mathcal{S} , ω_0 , and γ are the oscillator strength, frequency, and damping, respectively, and $\bar{n}(\omega)$ is the Bose population factor at frequency ω .

Results obtained at low temperature for the form of the expected magnetic Raman spectrum and its resolution into individual Raman peaks are shown in Fig. 1. The complicated Raman line shape can be resolved into six peaks arising from five peaks of magnetic origin and a phonon of E_{1g} symmetry. For the magnetic excitations of interest here (the quasi-1D ordered phase), we quote the experimental values obtained at temperatures between 12 and 25 K in Table I for reference.

III. THEORETICAL FORMALISM

As in the earlier work on RbCoCl₃ and similar quasi-1D antiferromagnets by Shiba [15,17] and Matsubara [4,16], among others, we may express the spin Hamiltonian in the form

$$\mathcal{H} = \sum_j \{2J_1[S_j^z S_{j+1}^z + \alpha_1(S_j^x S_{j+1}^x + S_j^y S_{j+1}^y)] + 2J_2[S_j^z S_{j+2}^z + \alpha_2(S_j^x S_{j+2}^x + S_j^y S_{j+2}^y)] + (-1)^j h S_j^z\}. \quad (2)$$

TABLE I. Frequencies of the magnetic excitations near zero wave vector observed using Raman spectroscopy for the quasi-1D phase in RbCoCl₃. The average value (and standard deviation) for each excitation over the 12 < *T* < 25 K temperature range is also given.

Magnon mode	Frequencies (cm ⁻¹) for 12 < <i>T</i> < 25 K	Average value (cm ⁻¹)	Standard deviation (cm ⁻¹)
1	90.0, 89.9, 90.3, 89.7, 90.0, 90.0, 90.3, 89.8, 89.7, 89.8	89.9	0.2
2	95.6, 95.7, 95.9, 95.6, 95.8, 96.0, 96.1, 95.7, 95.9, 95.9	95.8	0.2
3	98.9, 99.0, 99.3, 98.8, 99.1, 99.1, 99.2, 98.7, 99.0, 98.9	99.0	0.2
4	101.3, 101.5, 101.8, 101.2, 101.8, 101.4, 101.3, 100.9, 101.2, 101.2	101.4	0.3
5	110.2, 110.2, 110.5, 110.0, 110.4, 110.5, 110.8, 110.4, 110.7, 110.8	110.5	0.3

Here J_1 and J_2 are nearest-neighbor and next-nearest-neighbor Ising exchange interactions along a chain of Co⁺⁺ ions, while j labels the sites along the chain. The constants α_1 and α_2 specify the small degree of admixture of XY -type exchange in each case. The term h represents the magnitude of a staggered effective field (alternating in sign) acting at each site on a chain; it is attributed to the small interchain exchange. There is no single-ion anisotropy because the effective spin $S = \frac{1}{2}$ in this material. There could also be dipole-dipole contributions to the anisotropy. Values for these effective Hamiltonian parameters are fairly well known, with the possible exception of h , from the recent INS studies [18,19].

The theoretical background is briefly as follows. States with a single reversal (extendible to multiple reversals) of spins in an otherwise Néel-aligned antiferromagnetic chain may be considered, following [14,15,17]. We take N ($\rightarrow \infty$) as the number of spins along the chain, so there are $N/2$ on each sublattice. We can form a $\Delta S^z = \pm 1$ excitation by (for example) reversing one down-spin, or generally any odd number of adjacent spins starting from a down-spin. In effect, the hierarchy of such states is like creating a pair of domain walls (or soliton-like features). There are two Néel states, which we can denote as ψ_{N1} and ψ_{N2} according to whether site j is initially down or up, respectively. A single reversal is described by $S_j^+ \psi_{N1}$, which generalizes to

$$\psi_1(k) = \sqrt{\frac{2}{N}} \sum_k \exp(ikz_j) S_j^+ \psi_{N1}, \quad (3)$$

where k denotes the wave vector along the chain. Reversals of three adjacent spins, starting from any site, also represent a $\Delta S^z = \pm 1$ excitation and can be treated similarly, as can spin reversals from ψ_{N2} .

The magnon state will be a linear combination of the $|k, \nu\rangle \equiv \psi_{2\nu-1}(k)$ states for integer $\nu = 1, 2, \dots$. It follows, therefore, that the eigenvalues of the matrix $\langle k, \nu | \mathcal{H} | k, \nu \rangle$ will yield the energy spectrum. The expressions obtained for the matrix elements of the Hamiltonian, when effects of the exchange terms J_1 and J_2 and the staggered field h are included (as in [4,17]), are approximately

$$\langle k, \nu | \mathcal{H} | k, \nu \rangle = \begin{cases} 2J_1 - 2(1 - \alpha_2)J_2 + 2h & (\nu = 1), \\ 2J_1 - 4J_2 + 2(2\nu - 1)h & (\nu > 1), \end{cases} \quad (4)$$

for the diagonal ($\nu' = \nu$) matrix elements. Also $\langle k, \nu | \mathcal{H} | k, \nu' \rangle = 2\alpha_1 J_1$ with $\nu' = \nu \pm 1$ for the dominant off-diagonal elements. Here we have put $k \approx 0$ appropriate to the long wavelengths in Raman scattering, and we neglected terms of order $(\alpha_1)^2$ because $|\alpha_1| \ll 1$ in RbCoCl₃.

It is known generally that the Raman intensity $I(\omega)$ for scattering from a magnon of frequency ω is proportional to a dynamic spin-spin correlation function [20], or equivalently to the imaginary part of a Green's function of the form $G(S_k^+; S_k^-; \omega)$ at wave vector $k \approx 0$. In principle, this quantity, along with its poles at the magnon frequencies, can be found from the above Hamiltonian matrix, which takes a tridiagonal form when the above approximations are made. The interchain interactions (occurring when $h \neq 0$) enter only into the diagonal elements, exhibiting the so-called Zeeman ladder of values that increase with the index ν .

First, it is of interest to examine the results for the eigenvalues in the special case when $h = 0$; then the diagonal matrix elements, with the exception of the (1,1) element, take a fixed value. We can write

$$\omega \mathbf{I} - \mathcal{H} = \begin{pmatrix} d + \Delta & -2\alpha_1 J_1 & 0 & 0 & \dots \\ -2\alpha_1 J_1 & d & -2\alpha_1 J_1 & 0 & \dots \\ 0 & -2\alpha_1 J_1 & d & -2\alpha_1 J_1 & \dots \\ 0 & 0 & -2\alpha_1 J_1 & d & \dots \\ \vdots & \vdots & \vdots & \vdots & \ddots \end{pmatrix}, \quad (5)$$

where \mathbf{I} is the unit matrix, $d = 2J_1 - 4J_2$, and the difference term $\Delta = 2(1 + \alpha_2)J_2$. The combination $(\omega \mathbf{I} - \mathcal{H})$ is useful because, following [15], the spectral intensity $I(\omega)$ appropriate to RbCoF₃ at $k \approx 0$ can be found from

$$I(\omega) = f \text{Im}[(1 - 2\alpha_1)G(1, 1) - 2\alpha_1 G(1, 2)] + O(\alpha_1^2). \quad (6)$$

Here f is a proportionality factor and the Green's functions $G(i, j)$, with i and j denoting positive integers, are just the (i, j) matrix elements of the inverse $(\omega \mathbf{I} - \mathcal{H})^{-1}$. To proceed, we note that perturbed tridiagonal matrices having the same general form of Eq. (5) occur for magnons in other systems, e.g., in the evaluation of the spin-spin Green's functions for semi-infinite Heisenberg ferromagnets [23], or in the lattice dynamics of phonons [24]. By analogy, the Green's functions

are [23]

$$G(\nu, \nu') = \frac{1}{x - x^{-1}} \left\{ x^{\nu+\nu'} \left(\frac{1+x^{-1}\Delta}{1+x\Delta} \right) - x^{\nu-\nu'} \right\}, \quad (7)$$

where x is a complex parameter defined by $x + x^{-1} = d - \omega$ with $|x| \leq 1$. Using this result with Eq. (6) we find

$$I(\omega) = -\frac{1}{2\alpha_1 J_1} f \operatorname{Im} \left[\frac{(1-2\alpha_1)x - 2\alpha_1 x^2}{1+x\Delta} \right]. \quad (8)$$

This expression can have two types of imaginary parts. One arises when x lies on the unit circle ($|x| = 1$) in the complex plane. In this case, putting $x = e^{i\phi}$ where ϕ is a phase angle, we obtain the contribution

$$I_C(\omega) = \frac{1}{2J_1\alpha_1(1+d\Delta+\Delta^2)} \{ [(1-2\alpha_1)\sin\phi - 2\alpha_1\sin 2\phi] \times (1+\Delta\cos\phi) - \Delta\sin\phi[(1-2\alpha_1)\cos\phi - 2\alpha_1\cos 2\phi] \}, \quad (9)$$

provided the frequency ω lies in the range from ω_{C-} (when $\phi = \pi$) to ω_{C+} (when $\phi = 0$), denoting $\omega_{C\pm} = 2J_1(1 \pm 2\alpha_1) - 4J_2$. This can be identified with the expected continuum region of scattering, by analogy with [4,15]. The second way in which an imaginary part on the right-hand side of Eq. (8) can be obtained is if the denominator term $(1+x\Delta)$ vanishes. Then we can use the identity $1/(z+i0^+) = P(1/z) - i\pi\delta(z)$, where 0^+ is a positive infinitesimal and P indicates a principal value. After some lengthy algebra, we find there is a delta-function contribution given by

$$I_B(\omega) = \frac{\pi(\Delta^2 - 1)}{\Delta^3} [(1-2\alpha_1)\Delta + 2\alpha_1]\delta(\omega - \omega_B). \quad (10)$$

This occurs when $x = -1/\Delta$, which gives a necessary existence condition (from the definition of x) that $\Delta > 1$, or equivalently $|J_2| > \alpha_1 J_1 / (1 + \alpha_2)$. The corresponding bound magnon frequency ω_B is split off below the magnon continuum, where

$$\omega_{C-} - \omega_B = 2J_1\alpha_1[(\Delta - 1)^2/\Delta]. \quad (11)$$

We note that both the intensity contribution and the split-off frequency tend to zero as $\Delta \rightarrow 1$ from above, so it is a consequence of $|J_2|$ being sufficiently large. The intensity contribution we have obtained here analytically was previously discussed by numerical methods in [16]. We will show in the next section that the delta-function spike identifies well with an observed feature in the magnon Raman spectrum of RbCoCl_3 .

Next the inclusion of the staggered field h into the analysis is considered. It follows from Eq. (4) and our earlier discussion that the diagonal elements in the $(\omega I - \mathcal{H})$ matrix quoted in Eq. (5) become stepwise incremented (the Zeeman ladder studied in [4,17]) by an amount $2(2\nu - 1)h$ for the ν th term. An analytic solution is no longer feasible when $h \neq 0$, but the lowest several discrete eigenvalues of this dynamical matrix can be found numerically by truncating that dimension of the matrix to a large finite value M such that $M \gg 2J_1/h$. In practice, taking $M = 100$ is satisfactory for the parameter values of RbCoCl_3 , although we also employed larger values as a check. The discrete magnon modes occur for

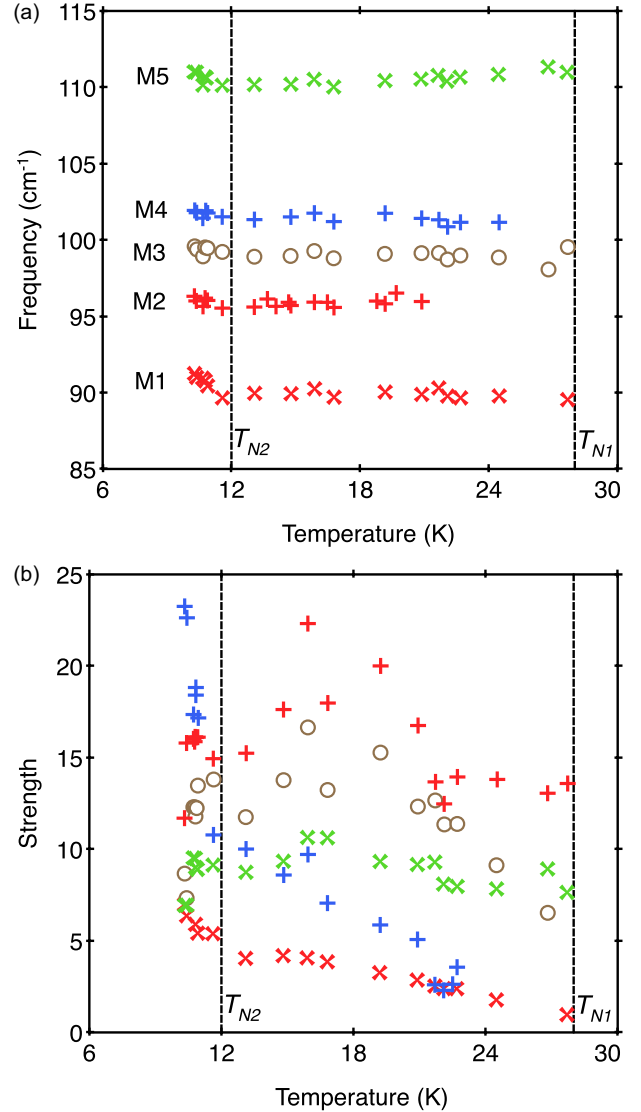


FIG. 2. (a) Temperature dependence of the frequencies of the magnon modes, M1 to M5, as obtained from the Raman scattering data with $T < T_{N1}$. (b) The corresponding temperature dependence of the strength factors \mathcal{S} of the magnons, where we use the same symbols for the data points.

$\omega > \omega_{C-}$ and extend above ω_{C+} . The results applied to the Raman data for RbCoCl_3 are presented in the next section.

IV. ANALYSIS OF THE MAGNON MODES

We already showed in Fig. 1 the overall form of the magnon Raman spectrum, where five magnon peaks were observed at low temperatures. More details for the measured temperature dependence of their frequencies and strength factors, as defined in Eq. (1), are given in Figs. 2(a) and 2(b), respectively. The data, which extend from just below the lower critical temperature T_{N2} up to the higher critical temperature T_{N1} , show little temperature variation for the magnon frequencies in these ordered regimes. The magnetic excitation energies are essentially independent of temperature between T_{N1} and T_{N2} , as can be seen in Fig. 2(a) and in

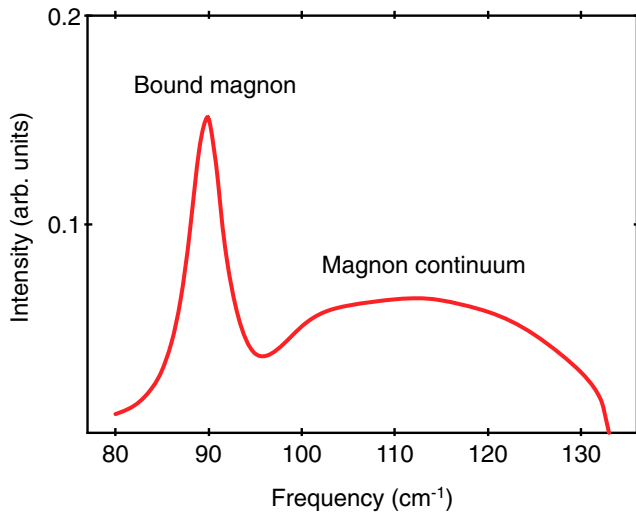


FIG. 3. The predicted Raman intensity plotted versus frequency in the case where the effects of the staggered field are neglected ($h = 0$), showing the bound magnon (represented by a Lorentzian) and the magnon continuum. See the text for further explanation.

Table I. By contrast, the magnon strengths show a significant overall decrease as T_{N1} is approached. There are no data shown above T_{N1} because the strength factors decrease sharply and/or the damping becomes too large, as would be expected for the magnons. For the purposes of comparing theory with experiment, we shall take $\omega_{M1} \simeq 90.5 \text{ cm}^{-1}$, $\omega_{M2} \simeq 96.0 \text{ cm}^{-1}$, $\omega_{M3} \simeq 99.0 \text{ cm}^{-1}$, $\omega_{M4} \simeq 102.0 \text{ cm}^{-1}$, and $\omega_{M5} \simeq 110.5 \text{ cm}^{-1}$ as the approximate average values applicable below T_{N2} . For the magnetic parameters of RbCoCl_3 , it was estimated in the recent INS data [18,19] that $J_1 = 5.89 \text{ meV} \equiv 47.51 \text{ cm}^{-1}$, $J_2 = -0.518 \text{ meV} \equiv -4.18 \text{ cm}^{-1}$, $\alpha_1 = 0.112$, and $\alpha_2 = 0.605$. The staggered field can take the possible values $2J_{NN}$, $4J_{NN}$, and $6J_{NN}$, where $J_{NN} \sim 1.0 \text{ cm}^{-1}$ is a single nearest-neighbor interchain exchange interaction [18,19]; this parameter value is probably more uncertain than the others.

First we discuss the predicted results when the weak interchain interactions are neglected. From the previous section we expect a delta-function spike (the bound magnon) split off from a magnon continuum region. Note that the deduced criterion for the existence of a bound magnon is satisfied, yielding a frequency $\omega_B \simeq 90.0 \text{ cm}^{-1}$. This is a close match to the observed magnon M1. Also we have $\omega_{C-} \simeq 90.5 \text{ cm}^{-1}$ and $\omega_{C+} \simeq 133.0 \text{ cm}^{-1}$ for the limits of the continuum. The intensity spectrum obtained using Eqs. (9) and (10) is shown in Fig. 3, where the delta-function contribution of the bound magnon has been represented by a Lorentzian line shape with a width chosen as 4.8 cm^{-1} (matching that found for the M1 peak in Fig. 1). We see that $|J_2|$ is sufficiently large in this case that the bound magnon is a strong feature overall.

When the weak staggered field is taken into account, the continuum part of the spectrum becomes discretized. We have calculated the modified eigenvalues for the magnon frequencies as a function of h , following the description in the previous section. The results are shown in Fig. 4 (see the red curves), where we also show the Raman magnon frequencies

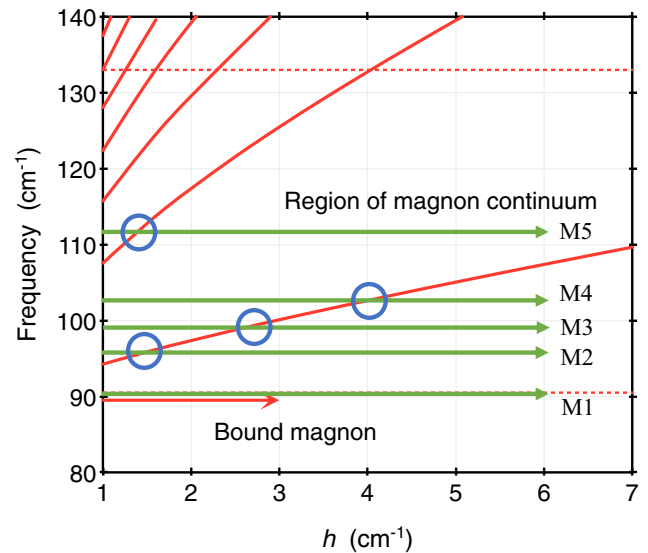


FIG. 4. Fits for the magnon modes $\{M1, M2, \dots, M5\}$ (red lines) to the predicted magnon bound state and the Zeeman ladder of the frequencies plotted versus the staggered field h . The horizontal solid lines (green in the online version) show the Raman frequencies at temperatures below T (see the text). The horizontal dotted lines indicate the boundaries of the magnon continuum region.

(horizontal green lines). This type of plot can be used to test the consistency of the Zeeman ladder theory and to make an estimate for the interchain exchange J_{NN} : we show by the blue circles the points of intersection between the horizontal lines representing the experimental frequencies and the red curves from theory. These points occur for $h \sim 1.4 \text{ cm}^{-1}$ (for M2 and M5), for $h \sim 2.8 \text{ cm}^{-1}$ (for M3), and for $h \sim 4 \text{ cm}^{-1}$ (for M4). Remarkably, the h values are seen to be in the correct approximate ratio $1 : 2 : 3$ to represent $2J_{NN}$, $4J_{NN}$, and $6J_{NN}$, giving us an estimate of $J_{NN} \sim 0.7 \text{ cm}^{-1}$. We note that this has a similar magnitude to the approximate value of 1.0 cm^{-1} quoted on the basis of the INS data [18,19]. We have therefore successfully accounted for the five observed Raman magnons in RbCoCl_3 , with one as a bound magnon state and the other four as Zeeman-ladder magnons. Very similar fits are obtained if the average magnon frequencies measured in the range from T_{N2} to T_{N1} are employed for the analysis.

V. CONCLUSIONS

In conclusion, by utilizing the latest structural and dynamical information obtained from the recent neutron scattering study of RbCoCl_3 [18,19] we have been able to formulate a fresh approach to interpreting the magnetic excitations observed at near-zero wave vector using Raman spectroscopy. Our approach is based broadly on the previous theoretical models that were developed to describe the characteristics of the magnon continuum, but we have presented an analytic extension to estimate the frequency and relative intensity associated with a bound magnon mode split off at a frequency just below the continuum region. This expected magnon bound state together with the underlying continuum of states

provided an excellent fit between the theory and one of the observed Raman magnons. With our model and the extension based on the Zeeman ladder approach, we found that the other magnetic features in the experimental data could be fitted with just one adjustable parameter (h) that proved to lie within the expected range. Hence the bound magnon and all of the other four magnons observed in the low-temperature phases of RbCoCl_3 are well predicted.

Finally, we note that the far-infrared spectroscopy measurements at high magnetic fields [9] in RbCoCl_3 led to magnon frequencies that are consistent (when extrapolated to zero field) with the Raman data, and thus can be accounted for theoretically. In fact, it can be inferred from [9] that there is another higher-frequency magnon at about 123 cm^{-1} . A fairly good fit for this extra mode is provided by the next curve

(or rung) on the Zeeman ladder when $h \sim 1.4 \text{ cm}^{-1}$. Such remarkable theoretical results are encouraging for the application of this theory to other analogous quasi-one-dimensional compounds as well as a basis for the development of a model for explaining the three-dimensional ferromagnetic ordering that occurs for RbCoCl_3 at temperatures below T_{N2} .

ACKNOWLEDGMENTS

We gratefully acknowledge support from the Natural Sciences and Engineering Research Council (NSERC) of Canada through Grant No. RGPIN-2017-04429. We also thank I. W. Johnstone (Co^{2+} -ion energy level schemes), H. J. Labbe (technical assistance), and B. Briat (samples) for their special contributions to the Raman work in [7].

-
- [1] H. Yoshizawa, K. Hirakawa, S. K. Satija, and G. Shirane, *Phys. Rev. B* **23**, 2298 (1981).
 - [2] S. E. Nagler, W. J. L. Buyers, R. L. Armstrong, and B. Briat, *Phys. Rev. B* **27**, 1784 (1983).
 - [3] W. Lehmann, W. Breitling, and R. Weber, *J. Phys. C: Solid State Phys.* **14**, 4655 (1981).
 - [4] F. Matsubara, S. Inawashiro, and H. Ohhara, *J. Phys.: Condens. Matter* **3**, 1815 (1991).
 - [5] J. P. Goff, D. A. Tennant, and S. E. Nagler, *Phys. Rev. B* **52**, 15992 (1995).
 - [6] S. E. Nagler, W. J. L. Buyers, R. L. Armstrong, and B. Briat, *Phys. Rev. Lett.* **49**, 590 (1982).
 - [7] D. J. Lockwood, I. W. Johnstone, H. J. Labbe, and B. Briat, *J. Phys. C: Solid State Phys.* **16**, 6451 (1983).
 - [8] D. J. Lockwood, in *Magnetic Excitations and Fluctuations*, edited by S. W. Lovesey *et al.* (Springer, Heidelberg, 1984), p. 33.
 - [9] R. Jörke and U. Dürr, *J. Phys. C: Solid State Phys.* **16**, L1129 (1983).
 - [10] A. Oosawa, Y. Nishiwaki, T. Kato, and K. Kakurai, *J. Phys. Soc. Jpn.* **75**, 015002 (2006).
 - [11] S. E. Nagler, W. J. L. Buyers, R. L. Armstrong, and B. Briat, *Phys. Rev. B* **28**, 3873 (1983).
 - [12] I. W. Johnstone, D. J. Lockwood, and M. W. C. Dharma-wardana, *Solid State Commun.* **36**, 593 (1980).
 - [13] D. J. Lockwood and I. W. Johnstone, *J. Appl. Phys.* **53**, 8169 (1982).
 - [14] J. Villain, *Physica B+C* **79**, 1 (1975).
 - [15] N. Ishimura and H. Shiba, *Prog. Theor. Phys.* **63**, 743 (1980).
 - [16] F. Matsubara and S. Inawashiro, *J. Phys. Soc. Jpn.* **58**, 4284 (1989).
 - [17] H. Shiba, *Prog. Theor. Phys.* **64**, 466 (1980).
 - [18] M. Mena, N. Hänni, S. Ward, E. Hirtenlechner, R. Bewley, C. Hubig, U. Schollwock, B. Normand, K. W. Kramer, D. F. McMorrow, and C. Ruegg, *Phys. Rev. Lett.* **124**, 257201 (2020).
 - [19] N. P. Hänni, D. Sheptyakov, M. Mena, E. Hirtenlechner, L. Keller, U. Stuhr, L. P. Regnault, M. Medarde, A. Cervellino, C. Ruegg, B. Normand, and K. W. Krämer, *Phys. Rev. B* **103**, 094424 (2021).
 - [20] M. G. Cottam and D. J. Lockwood, *Light Scattering from Magnetic Solids* (Wiley, New York, 1986).
 - [21] I. W. Johnstone and L. Dubicki, *J. Phys. C: Solid State Phys.* **13**, 4531 (1980).
 - [22] I. W. Johnstone, G. D. Jones, and D. J. Lockwood, *Solid State Commun.* **39**, 395 (1981).
 - [23] M. G. Cottam, *J. Phys. C: Solid State Phys.* **9**, 2137 (1976).
 - [24] P. Mazur and A. A. Maradudin, *Phys. Rev. B* **24**, 2996 (1981).